Research paper

Simulation and optimization of a liquid organic hydrogen carrier based hydrogen train system

Christoph Regele [a], Felix Gackstatter [a], Florian Ortner [a], Patrick Preuster [b,c], Michael Geißelbrecht [a],*

[a] *Forschungszentrum Jülich, Helmholtz Institute Erlangen-Nürnberg for Renewable Energy (IET-2), Cauerstr. 1, 91058 Erlangen, Germany*
[b] *Rosenheim Technical University of Applied Sciences, Faculty of Chemical Technology and Economics, Marktler Straße 50, 84489 Burghausen, Germany*
[c] *Fraunhofer IEG, Fraunhofer Research Institution for Energy Infrastructure and Geothermal Systems IEG, Am Hochschulcampus 1, 44801 Bochum, Germany*

ARTICLE INFO

ABSTRACT

The transition of the transport sector from fossil fuels to carbon dioxide free technologies is an enormous challenge. Liquid organic hydrogen carrier (LOHC) fueled trains are an attractive option for all non-electrified railway lines currently operated by diesel trains. The driving unit of a LOHC fueled train consists of LOHC storage tanks, a hydrogen release unit, a heating unit, a fuel cell and a battery. In our study, the LOHC system dibenzyl toluene/perhydro-dibenzyl toluene is selected. The dimensioning of the individual units is not straightforward as a smaller battery would require a larger fuel cell and the choice of a fuel cell influences the size of the heating unit, as the waste heat from a solid oxide fuel cell (SOFC) can be used for the dehydrogenation process. However, a SOFC of the same power class is larger and heavier than a proton exchange membrane fuel cell (PEMFC) and reduction of the size of the heating unit can result in an increase of the fuel cell size. By using a genetic optimization algorithm, we can minimize volume, mass and total driving costs of the model-based driving unit. The optimized driving unit contains a 722 kW fuel cell, a 820 kW$_{LHV-H2}$ hydrogen release unit and a 523 kWh battery. This configuration results in a volume around 45 m^3, a total mass around 27 t and driving costs around 3 EUR/km for the SOFC scenario and 60 m^3, 26 t and 2.4 EUR/km for the PEMFC scenario.

1. Introduction

The railway sector is considered to play a major role in decarbonizing the future global transport sector, which causes 15.5% of global greenhouse gas (GHG) emissions [1,2]. GHG emissions can be decreased by shifting capacities from the road sector to the railway sector as the railway sector has a better energy efficiency (per passenger-km) than the road sector and hence lower GHG emissions [3]. However, GHG emissions remain. In order to meet the expected increase in demand in the rail sector and at the same time reduce greenhouse gas emissions, emission-free propulsion technologies are therefore required for rail transportation. There are several options for this, all of which are based on the complete electrification of the propulsion unit. The most common approach is the direct usage of electricity via catenary. Currently less than 30% of worldwide routes are electrified and therefore still many diesel driven trains are in operation, which also pose a health hazard because of carbon monoxide, nitrogen oxides and particulate matter emissions [4,5]. This can be explained by the fact that on some routes electrification makes no sense from an economic point of view due to high investment costs and long construction times. On those routes two alternatives have emerged in the last years, battery electric and fuel cell electric trains [6]. Battery electric trains are suited for operation on shorter routes, while fuel cell powered trains are considered to offer comparable ranges like conventional diesel driven trains while maintaining fast refueling times [7]. Nevertheless, the deployment of hydrogen trains also bears some challenges. The low volumetric energy density of hydrogen at ambient conditions compared to diesel is a drawback but can be overcome by various options. These options are normally divided into physical and material-based technologies [8].

The first one comprises compressed gas hydrogen, cold-compressed hydrogen, liquid hydrogen and cryo-compressed hydrogen. According to Böhm et al. the 35 MPa compressed gas storage technology is the state of the art for the railway sector, since liquid hydrogen still has long term storage problems and cryo-compressed hydrogen is currently at a low technology readiness level. However, the current standard cannot reach the final DOE (Department of Energy, America) targets.

Nomenclature

α_{shell}	Shell-side heat transfer coefficient (W/(m^2 · K))
α_{tube}	Tube-side heat transfer coefficient (W/(m^2 · K))
ΔT	Temperature difference (K)
η_{bat}	Battery efficiency (−)
η_{ch}	Battery charging efficiency (−)
$\eta_{DC,AC}$	Power electronics efficiency (−)
η_{disch}	Battery discharging efficiency (−)
η_{FC}	Fuel cell efficiency (−)
η_{motor}	Motor efficiency (−)
λ	Rotary allowance factor (−)
ν_k	Stoichiometric coefficient of component k (−)
τ_i	Residence time in cascade element i (s)
a	Acceleration (m/s^2)
$ACAPEX_{exchange}$	Annualized capital expenditure for exchange (EUR/a)
$ACAPEX_{tot}$	Annualized total capital expenditure (EUR/a)
AF	Annuity factor (−)
C	Constant (kg/m^3)
$CAPEX_{exchange}$	Capital expenditure for exchange (EUR)
$CAPEX_{tot}$	Total capital expenditure (EUR)
$c_{H18-DBT}$	Concentration of H18-DBT (mol/m^3)
$c_{H18-DBT,0}$	Concentration of H18-DBT at start of reaction (mol/m^3)
$c_{p,steel}$	Heat capacity of steel (J/(kg · K))
$DoDH_{eq}$	Degree of dehydrogenation at equilibrium (−)
E_A	Activation energy (kJ/(mol · K))
$E_{bat,max}$	Maximum energy content of battery (Wh)
E_{train}	Overall train energy demand (J)
$E_{train,prop}$	Train energy demand for propulsion (J)
F_a	Acceleration force (N)
F_{tr}	Tractive force (N)
$h_{LOHC,in}$	Specific enthalpy of LOHC inlet flow (J/kg)
$h_{LOHC,out}$	Specific enthalpy of LOHC outlet flow (J/kg)
k_0	Reaction rate constant (m^3/(kg · s))
K_{eq}	Equilibrium constant (−)
LHV	Lower Heating Value (J/kg)
$m_{LOHC,init}$	Initial LOHC mass (kg)
$m_{battery}$	Battery mass (kg)
m_{cat}	Catalyst mass (kg)
$m_{fuelcell}$	Fuel cell mass (kg)
$m_{H2burner}$	Hydrogen burner mass (kg)
$\dot{m}_{H2,fc}$	Hydrogen massflow (fuel cell) (kg/s)
M_k	Molar mass of component k (g/mol)
$\dot{m}_{HM}$	Mass flow of heating medium (kg/s)
$\dot{m}_{H2,reactor}$	Hydrogen massflow (reactor) (kg/s)
m_{H2tank}	Hydrogen tank mass (kg)
$\dot{m}_{k,i}$	Change in mass flow rate for the component k in cascade element i (kg/s)
$\dot{m}_{LOHC}$	LOHC mass flow (reactor inlet) (kg/s)
$m_{LOHCtanks}$	LOHC tank mass (kg)
m_{LOHC}	LOHC mass inside of tank (kg)
$\dot{m}_{LOHC,in}$	LOHC inlet mass flow (kg/s)
$\dot{m}_{LOHC,out}$	LOHC outlet mass flow (kg/s)
M_{pass}	Passenger mass (kg)
$m_{pt,tot}$	Total powertrain mass (kg)
$m_{reactor}$	Reactor mass (kg)
$m_{steel,reactor}$	Reactor steel mass (kg)
$M_{train,eff}$	Effective train mass (kg)
$M_{train,tare}$	Train tare mass (kg)
n	Depreciation period (a)
OM_{tot}	Total operation and maintenance costs (EUR/a)
$OPEX_{elec}$	Operational expenditure for electricity (EUR/a)
$OPEX_{LOHC,H2}$	Operational expenditure for LOHC (EUR/a)
$P_{Aux,DC}$	Auxiliary power demand (W)
P_{bat}	Battery power (W)
P_{FC}	Current fuel cell system power (W)
$P_{FC,rated}$	Rated fuel cell power (W)
P_{H2}	Thermal hydrogen power (W)
PLR	Part Load Ratio (−)
P_{train}	Train power demand at wheel (W)
$P_{train,DC}$	Overall train power demand (W)
$\dot{Q}$	Heat flow (W)
R	General gas constant (J/(K · mol))
r	Reaction rate (mol/(m^3 · s))
REV_{elec}	Revenues for fed-in electricity (EUR/a)
SOC	State of charge (−)
SOC_{init}	Initial state of charge (−)
s_{year}	Yearly covered distance (km)
T_{HM}	Heating medium temperature (K)
u	Specific internal energy (J/kg)
$V_{battery}$	Battery volume (m^3)
$V_{fuelcell}$	Fuel cell volume (m^3)
$V_{H2burner}$	Hydrogen burner volume (m^3)
$V_{H18-DBT}$	Fluid volume (m^3)
V_{H2tank}	Hydrogen tank volume (m^3)
$\dot{V}_{Hx-DBT,i}$	Volume flow of Hx-DBT (m^3/s)
$c_{v,LOHC}$	Isochoric LOHC heat capacity (J/(kg · K))
$V_{LOHCtanks}$	LOHC tanks volume (m^3)
$V_{pt,tot}$	Total powertrain volume (m^3)
$V_{reactor}$	Reactor volume (m^3)
v_{train}	Train speed (m/s)
$WACC$	Weighted average cost of capital (−)
w_{EM}	Precious metal mass fraction on the catalyst (−)
X_{pen}	Penalty (−)

Therefore, the second category, material-based technologies, could be viable options, which could accelerate and facilitate the establishment of hydrogen trains [8,9].

According to Xu et al. who reviewed several hydrogen storage options for the railway sector, Liquid Organic Hydrogen Carriers (LOHC) could be used in the future due to their high hydrogen capacity and relatively low costs. Furthermore, together with ammonia (direct combustion) they offer the highest technology readiness level in the field of chemical storage methods [9]. Lee et al. compared the energy demand for the hydrogen supply chain for the hydrogen storage vectors

liquified hydrogen, ammonia, LOHC and methanol. Liquified hydrogen has the lowest total energy demand, followed by methanol, LOHC, and ammonia. However, LOHC has the lowest electricity demand, which enables a huge reduction in energy demand if waste heat from other processes can be used for heat provision [10]. The concept of LOHCs is based on binding the hydrogen to an organic molecule via a heterogeneously catalyzed reaction (hydrogenation) and releasing it again via an endothermic, heterogeneously catalyzed reaction (dehydrogenation). Due to its properties, the LOHC storage system can be handled, transported and stored in large quantities in both hydrogenated and dehydrogenated form at ambient conditions, just like today's liquid fuels. In the past few years, various chemical substances have been discussed for use as carrier materials, each with slightly different properties [11–13]. One commonly used system is dibenzyl toluene (H0-DBT)/perhydro-dibenzyl toluene (H18-DBT) with a hydrogen capacity of up to 6.2 wt%. This system offers high availability since it has been widely used as heat transfer fluid in industry, e.g. under the trade name Marlotherm SH. Furthermore, its high boiling point (390 °C for H0-DBT) reduces the purification effort for the released hydrogen and enables liquid phase dehydrogenation, which is beneficial for the stability of the used catalyst [14,15].

In terms of heat supply for the dehydrogenation Müller et al. investigated several scenarios. Electric heating turned out to be the least favorable option, since an LOHC-bound hydrogen to electricity efficiency of only $13.6 \pm 9.7\%$ can be reached. The partial combustion of hydrogen on the other hand reaches efficiencies of $28.7 \pm 5.8\%$. However, the most efficient and hence technically most favorable approach with efficiencies of $48.1 \pm 9.6\%$ would be the coupling of a high-temperature fuel cell and the dehydrogenation process [16]. Preuster et al. demonstrated the waste heat integration of a solid oxide fuel cell (SOFC) into the dehydrogenation process. By minor adjustments in the preheating of the air supply for the SOFC the thermal energy demand of the dehydrogenation unit could be covered by the SOFC exhaust gas for different degrees of fuel utilization [17]. Combustion based waste heat usage was also already investigated. Dennis et al. have shown the potential for combining H18-DBT dehydrogenation with a hydrogen fired turbine [18]. Biswas et al. reported a significant reduction in hydrogen demand for the heat supply of LOHC dehydrogenation when the waste heat from a hydrogen combustion engine is used to heat the dehydrogenation reactor [19]. The possibility of the direct usage of the exhaust enthalpy of a porous media burner for the dehydrogenation of H18-DBT has been shown by Bollmann et al. The released hydrogen was at kW-scale (3.9 kW). They could also demonstrate the dynamic operation of the dehydrogenation reactor under varying LOHC mass flow rates, reaction temperatures and pressures, which has already been reported by Fikrt et al. in a different reactor design [20,21]. As dehydrogenation is an endothermal reaction with enormous heat demand, the heat transfer to the catalyst bed is crucial for the realization of a compact dehydrogenation unit [22,23]. Since the heat transfer in the catalyst bed is limited for a thermal oil heated fixed bed multi-tubular reactor, several alternative reactor configurations have been developed. Wunsch et al. developed a micro-structured reactor concept to intensify the heat transfer in the catalyst bed by increasing the heat transfer area [24]. Heat transfer to the catalyst can also be intensified by coating the reactor walls with a catalytically active layer [25]. Furthermore, the temperature gradient within the catalyst bed can be reduced by using a phase-change heat medium [26]. However, most alternative reactor configurations are still in the development phase, and a fixed-bed multi-tube reactor is the most mature technology.

Several publications showed the general applicability of the released hydrogen for reconversion to electricity in fuel cells. Geiling et al. demonstrated the combined continuous and dynamic operation of the dehydrogenation of H18-DBT and a proton exchange membrane fuel cell (PEMFC). The setup consisted of a 14 tubes containing tubular reactor, that was filled with a platinum catalyst supported on alumina oxide, several heat exchangers, filters (coalescence, activated carbon),

a small hydrogen buffer tank and a 25 kW PEMFC. A PI-controller can control the fuel cell power quickly by adapting the fuel cell current to the hydrogen release rate of the LOHC reactor. Furthermore, no stack degradation was detected after the operation of the fuel cell with hydrogen released from H18-DBT [27]. However, all the explained examples deal with stationary applications, whereas the application of LOHC technology in train systems has not been investigated in detail so far. Other areas of application in mobility have already been discussed for LOHC technology. The direct usage of LOHC bound hydrogen in a passenger car is not reasonable considering the current status of LOHC technology [28]. Biswas et al. proposed a design for a long-haul truck powered by LOHC with attractive economics [19]. Runge et al. evaluated the technical and economic feasibility of producing hydrogen or its derivatives at excellent locations and transporting it to Germany [29,30]. The hydrogen distribution using LOHC technology showed promising mobility costs, although hydrogen must be released and compressed at a filling station in order to be dispensed as compressed gas to the vehicle. The on-board dehydrogenation without the necessity to compress the released hydrogen would significantly reduce mobility costs and increase attractiveness of LOHC technology.

For compressed hydrogen-based train systems several publications exist, which deal with the investigation of different control systems of the trains and the analysis of the energy saving potential by dynamical simulation. Meegahawatte et al. did an analysis of potential carbon dioxide savings by replacing the standard powertrain of a Class 150 Diesel Multiple Unit railway vehicle by a hydrogen powertrain for different fuel cell sizes and control strategies on the route Stratford Upon Avon and Birmingham in UK [31]. They concluded that the fuel cell hybrid system can reduce carbon dioxide emissions by 45% compared to a pure diesel train. Hoffrichter et al. used the same route to compare the energy savings of a hydrogen and a hydrogen–hybrid powertrain with the standard diesel–electric powertrain of Stadler's Gelenktriebwagen 2/6 (GTW). One finding was that the hydrogen–hybrid system can achieve an energy consumption reduction of 55% [32]. In addition to these regional train analyses, there are also studies on the use of hydrogen in urban and freight trains [33–35]. The aforementioned analysis of the powertrain can also be combined with mathematical optimization approaches. Silvas et al. reviewed various approaches for the optimized dimensioning of hybrid electric vehicles in general. According to them there is no algorithm that can be applied universally for optimal system design. However, evolutionary algorithms, especially genetic algorithm (GA) and particle swarm optimization (PSO), seem to be used most frequently [36]. Sarma et al. used PSO for an optimization of the component's sizes of a fuel cell–battery hybrid system for an intercity passenger train on three different routes. Their goal was to minimize the total cost of the system while also comparing two energy management systems [37].

Overall, several studies have shown promising results in terms of the general usage of hydrogen in the railway sector. At the same time the material-based hydrogen storage approach of LOHCs has been named as a possible accelerator for hydrogen mobility. Based on these results the concept of a LOHC-based hydrogen train system will be investigated by means of dynamical simulation in this publication. This includes an optimized sizing of the main components of the powertrain system in terms of costs, mass and volume and for different topology and control scenarios on three different tracks by applying a genetic algorithm based multi-objective optimization.

2. Simulation approach

The general simulation approach can be divided into two parts, determination and optimization of the train speed profile and determination and optimization of the configuration of the powertrain. In the first part, various acceleration profiles were tested on the basis of artificial timetable assumptions for train and real route characteristics in order to generate an optimized power profile as input parameter

Table 1

Train simulation parameters.

Train characteristics	Value	Unit	Reference
Train tare mass	119.5	t	Own calculations, comparable with [39,40]
Number of passengers	160	–	Assumption based on [41]
Mass per passenger	75	kg	[42]
Maximum speed	150	km/h	Assumption due to limitation of F_{tr} eq.
Maximum power at wheel	1700	kW	Assumption based on [41]
Efficiency DC/AC	0.975	–	[32]
Efficiency motor/generator	0.95	–	[32]

for the second part. This part will not be discussed in detail in this publication, can however be found in the electronic supplementary information (ESI). Instead, the focus is on the second part, which deals with the optimized sizing of the powertrain components. This includes fuel cell, dehydrogenation system, battery and LOHC tanks. Furthermore, different control strategies are tested. Main input parameter for the powertrain optimization is the power profile of the first optimization. The modeling and simulation of the individual systems and the overall system is done in MATLAB Simulink. The subsequent optimization using GA is done using MATLAB's Global Optimization Toolbox.

2.1. Train dynamics

The calculation of the train's traction force and power demand is based on Newton's second law of motion, where F_a is the acceleration force (resistance), $M_{train,eff}$ is the effective train mass and a is the train acceleration. $M_{train,eff}$ includes a rotary mass, that considers the inertia of vehicle components via the rotary allowance factor λ, as well as the passenger mass M_{pass}. λ depends on the train type and is taken from literature. For complete trains a value of 0.08 is a good assumption according to Filipovic [38].

$$F_a = M_{train,eff} \cdot a \tag{1}$$

$$M_{train,eff} = M_{train,tare}(1 + \lambda) + M_{pass} \tag{2}$$

In order to determine the tractive force F_{tr} a balance of forces is made including all resisting forces. For more details see ESI. The resulting power can then be calculated by the multiplication of the tractive force by the current train speed.

$$P_{train} = F_{tr} \cdot v_{train} \tag{3}$$

Losses due to the electric motor and power electronics are taken into account through efficiencies (see Table 1).

$$P_{train,DC} = \frac{P_{train}}{\eta_{motor} \cdot \eta_{DC,AC}} \tag{4}$$

Table 1 gives references to electrical trains (three-car sets) with a similar driving power. The total mass of these trains is between 112–114 t. The weight of the train in our optimized dimensioning process was assumed to be constant (119.5 t) and is close to the reference. The constant weight is sufficient for the goal of our investigation as we want to give a first system design of a LOHC-fueled train, which can be optimized in future. Otherwise, a recalculation of the power profile would have been necessary in every iteration step of the optimization process.

2.2. Powertrain structure

A scheme of the powertrain of the LOHC-based hydrogen train system can be seen in Fig. 1. Three energy storage systems are used, the LOHC tank with H18-DBT, the lithium-ion battery and the hydrogen buffer volume, the latter being comparatively small. In terms of LOHC storage dual-use storage tanks are assumed. This means that tanks that supply the LOHC dehydrogenation reactor with hydrogenated LOHC

(H18-DBT) take up dehydrogenated LOHC (Hx-DBT) when they are empty. This approach requires only one additional (empty) tank at the beginning. The reactor system is defined as a multi-tubular reactor, which is scaled in the optimization process by numbering up of the tubes. Heat exchangers are used for transferring the heat of the products Hx-DBT and hydrogen to the feed consisting of H18-DBT but are not displayed separately in the block scheme due to simplification. Hydrogen is released in the reactor tubes containing the Pt-AlOx catalyst. The required heat is provided by a thermal oil flowing through the shell of the reactor system. The thermal oil cycle contains Marlotherm SH, a commercially available heating oil, which is heated externally either by a hydrogen burner or by the exhaust gas of the fuel cell in case of SOFC usage. Between reactor and fuel cell a small hydrogen buffer tank is used to balance potential deviations between the hydrogen consuming fuel cell and the hydrogen supplying reactor, e.g. in emergencies. However, these cases have not been investigated in detail. The target pressure of the buffer tank is 0.3 MPa. For an assumed number of five tanks this equals roughly 0.04 kg of hydrogen, when emptied to ambient pressure. As the dynamics of the fuel cell are faster than dynamics of the hydrogen release reactor, all supplied hydrogen can be consumed in the fuel cell. This allows constant pressure inside the buffer tank. The fuel cell converts the released hydrogen into electrical power to cover the power demand for the propulsion of the train as well as auxiliary power demand, e.g. for heating ventilation and air conditioning (HVAC). The battery has two functions namely, to cover power peaks, e.g. during acceleration, and to recuperate braking energy.

2.3. Train control

Due to its easy implementability the stateflow system approach is chosen to model the control system of the LOHC train and the reactor system. Its main purpose is to calculate the current battery power via a power balance. For the default state of the train when it is on the track, the following equation is used.

$$P_{bat,DC} = P_{trac,DC} + P_{aux,DC} - P_{FC,out,DC} \tag{5}$$

This involves the traction power $P_{trac,DC}$, the auxiliary power $P_{aux,DC}$ and the current fuel cell power $P_{FC,out,DC}$. The latter is defined by the hydrogen release rate of the reactor, as the fuel cell uses the amount of hydrogen released in the reactor minus the amount for the hydrogen burner. The reactor can be operated in two predefined operating states (see Section 2.7.2). In case of the recharging of the battery via grid a constant power of 200 kW is set for the battery power.

2.4. Fuel cell model

The implemented fuel cell model is based on an efficiency graph of a fuel cell system with a rated power of 90 kW (see Fig. 2) for the PEMFC and with a rated power of 200 kW for the SOFC system. The fuel cell system power P_{FC} equals the product of the fuel cell system efficiency η_{FC} and the thermal power of the fed hydrogen P_{H2}. η_{FC} can therefore also be expressed as the ratio of P_{FC} and P_{H2} [43]. P_{FC} takes into account several losses of the fuel cell at stack and system level. This includes voltage losses, losses due to incomplete fuel utilization and power losses of the stack due to auxiliary power demand (e.g. air blower). By expressing the hydrogen power using the lower
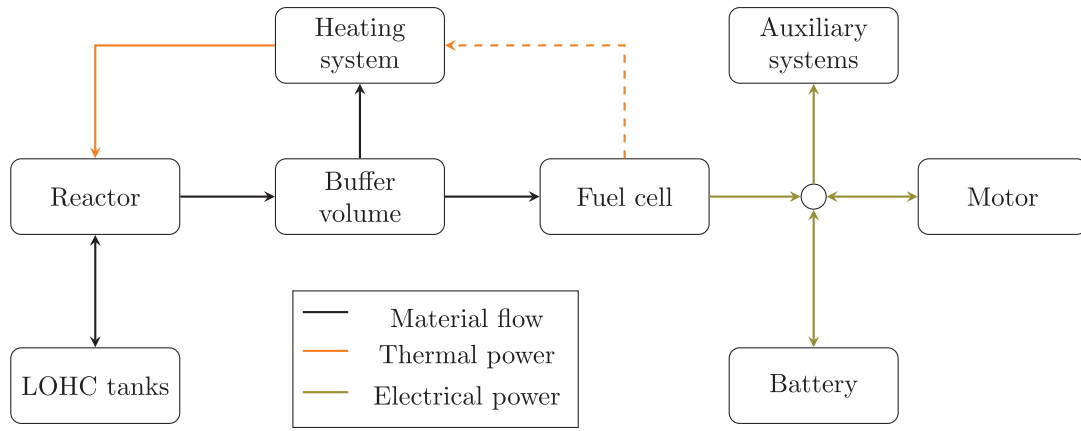
Fig. 1. Simplified block scheme of the powertrain of the LOHC-based hydrogen train.
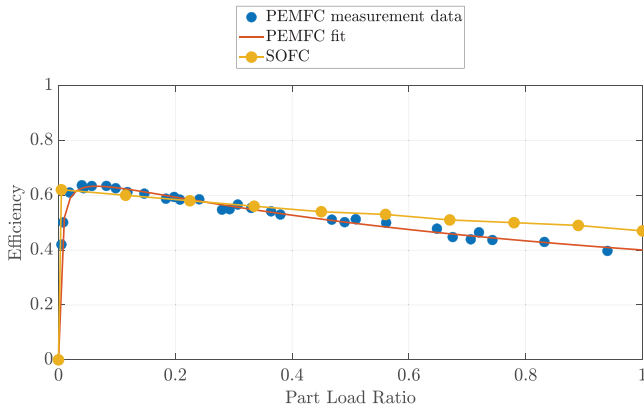

Fig. 2. Efficiency curves of PEMFC [44] and SOFC.

heating value of hydrogen LHV and the hydrogen mass flow $\dot{m}_{H2}$, the dependence of the hydrogen mass flow on the system power and vice versa can be shown. For easy scaling efficiency is normalized to the rated power, which gives the part load ratio (PLR) parameter. Thus, the fuel cell system efficiency and the resulting hydrogen demand can be determined for every PLR (0–1).

$$P_{FC} = \eta_{FC}(PLR) \cdot P_{H2} \tag{6}$$

$$P_{H2} = LHV \cdot \dot{m}_{H2,fc} \tag{7}$$

$$\dot{m}_{H2,fc} = \frac{P_{FC}}{LHV \cdot \eta_{FC}} \tag{8}$$

$$PLR = \frac{P_{FC}}{P_{FC,rated}} \tag{9}$$

2.5. Battery model

The implemented battery model is rather simple and often named "bucket model", since it can be compared to a bucket with a certain amount of energy [45]. The current "filling level" can be expressed by the state of charge (SOC) of the battery. It varies depending on the charging or discharging power P_{bat}. Losses are considered by charging and discharging efficiencies (η_{ch} and η_{disch}). The calculation of the SOC is based on the integration of the charging or discharging power, which is then divided by the maximum battery energy content. Multiplied with either the charging or discharging efficiency this equals the change of the SOC. In order to receive the current SOC, the SOC change is added to the initial state of charge SOC_{init}. The battery charging

efficiency η_{ch} is set to 0.98, while the battery discharging efficiency η_{disch} is set to 1.00 [46]. Degradation is neglected.

$$SOC(t) = \frac{\int_0^T \eta_{bat} \cdot P_{bat}\, dt + SOC_{init} \cdot E_{bat,max}}{E_{bat,max}} \tag{10}$$

$$\eta_{bat} = \begin{cases} \eta_{ch} & P_{bat} < 0, \\ \frac{1}{\eta_{disch}} & P_{bat} > 0. \end{cases} \tag{11}$$

2.6. Liquid organic hydrogen carrier tank model

The LOHC tank model is used either as feed or as product tank, as described in Section 2.2. It balances the mass of LOHC m_{LOHC} in a defined volume (see Eq. (12)), which includes the consideration of the resulting degree of hydrogenation (DoH) in case of the product tank. For more details on the DoH, see [14]. Therefore, in the case of the feed tank the initial LOHC mass and the outgoing mass flow are taken into account. For the product tank the incoming mass flow is integrated over time. Furthermore, the resulting temperature change of the liquid dT is calculated. This is done by applying an energy balance (see Eq. (13)). The required thermophysical properties of the investigated LOHC system are taken from [47]. For the geometry of the tanks a cube is assumed, since the application will be aboard the LOHC hydrogen train, where space has to be used efficiently. The dimensions are based on commercially available tanks with an inner volume of $1\,\mathrm{m}^3$ and an outer volume of $1.6\,\mathrm{m}^3$ [48]. The overall LOHC tank volume is scaled by increasing the number of LOHC tanks.

$$m_{LOHC} = m_{LOHC,init} + \int_0^T \dot{m}_{LOHC,in}\, dt - \int_0^T \dot{m}_{LOHC,out}\, dt \tag{12}$$

2.7. Reactor model

The reactor model for the dehydrogenation of H18-DBT is based on the approach by Peters et al. which is a continuous-stirred-tank reactor cascade [49]. In each segment of the cascade mass and energy balances are solved. This is done for the shell-side and the tube-side of the reactor. Some adjustments to the original model have been implemented. First, the kinetic expression for the dehydrogenation of H18-DBT has been replaced by the approach of Geißelbrecht et al. which is a power law approach, that considers the back and forward reaction [50]. The equation for the reaction rate r is therefore as follows.

$$r = k_0 \cdot C \cdot e^{\frac{-E_A}{RT}} \cdot c_{H18-DBT} - \frac{k_0}{K_{eq}} \cdot C \cdot e^{\frac{-E_A}{RT}} \cdot (c_{H18-DBT,0} - c_{H18-DBT}) \tag{14}$$

It contains the reaction rate constant k_0, activation energy E_A, general gas constant R, temperature T, concentration of H18-DBT $c_{H18-DBT}$,

$$\frac{dT}{dt} = \frac{\dot{Q} + \dot{m}_{LOHC,in} \cdot h_{LOHC,in} - \dot{m}_{LOHC,out} \cdot h_{LOHC,out} - u(\dot{m}_{LOHC,in} - \dot{m}_{LOHC,out})}{m_{LOHC} \cdot c_{v,LOHC}} \tag{13}$$

Box I.

concentration of H18-DBT at start of reaction $c_{H18-DBT,0}$, constant C and equilibrium constant K_{eq}. C contains the mass of the catalyst m_{cat}, the mass fraction of precious metal on the catalyst w_{EM} and the fluid volume $V_{H18-DBT}$.

$$C = \frac{m_{cat} \cdot w_{EM}}{V_{H18-DBT}} \tag{15}$$

K_{eq} is based on the degree of dehydrogenation at equilibrium $DoDH_{eq}$, which can be calculated according to the equation published by Dürr et al. [14].

$$K_{eq} = \frac{DoDH_{eq}}{1 - DoDH_{eq}} \tag{16}$$

The change in mass flow rate $\dot{m}_{i,R}$ occurring during the reaction in cascade element i for the component k (LOHC or hydrogen) is determined as follows.

$$\dot{m}_{k,i} = \nu_k \cdot \tau_i \cdot r_i \cdot \dot{V}_{Hx-DBT,i} \cdot M_k \tag{17}$$

Where ν_k is the stoichiometric coefficient of component k, τ_i is the residence time in cascade element i, r_i is the reaction rate in cascade element i, $\dot{V}_{Hx-DBT,i}$ is the volume flow of Hx-DBT in cascade element i and M_k is the molar mass of component k.

The second adjustment concerns the reactor geometry. The original reactor is a plate reactor that is heated by SOFC exhaust gas. In this application, as described in Section 2.2, a tubular reactor with multiple tubes with an inner diameter of 27.7 mm and a length of 1 m is used. It is heated by a thermal oil. As guidance for the design and the dimensions serves the reactor described by Geiling et al. [27]. The dehydrogenation takes place in the tubes containing the catalyst. Here a heat transfer coefficient of 350 W/(m² K) is used [49], whereas on the shell side a heat transfer coefficient of 351 W/(m² K) is used based on calculations according to VDI Wärmeatlas [51]. The reactor and therefore the hydrogen release capacity is scaled up by increasing the number of tubes. The parameters used can be seen in Table 2. Based on the described reactor model several combinations of input parameters have been tested, in order to generate a characteristic diagram, which is implemented as lookup table in the overall system due to simplification reasons. Since real world reactors do have some inertia concerning temperature and fluid dynamics, potential changes of operating points were considered by the implementation of a constant rate limiter, that leads to a linear increase or decrease. This affects the LOHC mass flow, because the change of operating points is done by a variation of this parameter (see Section 2.7.2). The value of the rate limiter (8.1×10^{-7} kg/s²) is based on the time needed until 90% of the hydrogen output of the new stationary operating point is reached after an LOHC increase. This time is abbreviated by t90. According to published data by Geiling et al. who evaluated the dynamic behavior of LOHC dehydrogenation via real-time measurements, t90 can be determined as 80 min [27].

2.7.1. Reactor operating points

Fig. 3 shows the results of the reactor simulations with different input parameters. The LOHC mass flow (H18-DBT) and the heating medium temperature were varied between 2 kg/h and 20 kg/h and 220 °C and 330 °C. The dots outlined in blue indicate the corresponding hydrogen release rate for a steady-state operating point with these input parameters. Out of these, the red filled dots are those with a DoH equal or smaller than 22%. This was set as the threshold for a potential eco mode operating point, in order to use more than 78% of the

Table 2
Thermophysical and reaction kinetic parameters of the unscaled reactor system.

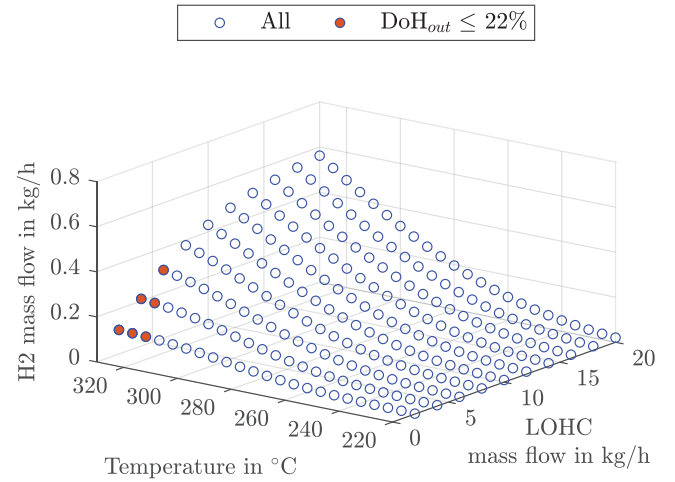| Parameter	Value	Unit	Reference
α_{shell}	351	W/(m² K)	Calculated [51]
α_{tube}	350	W/(m² K)	[49]
k_0	6.35×10^6	m³/(kg s)	[50]
E_a	109	kJ/(mol K)	[50]
w_{EM}	0.3	wt%	[50]
$\dot{m}_{HM}$	0.246	kg/s	Own estimation

Fig. 3. Characteristic diagram for the LOHC dehydrogenation reactor at 0.3 MPa containing the hydrogen release rate for variable heating medium temperatures and LOHC (H18-DBT) mass flow rates.

stored hydrogen. Out of those red filled dots the one with the highest hydrogen release rate was selected as operating point for eco mode ($\dot{m}_{LOHC}$ = 6 kg/h, T = 330 °C). Lower DoH limits might be possible by decreasing the LOHC mass flow rate while maintaining the heating medium temperature. However, decreasing the mass flow to 2 kg/h would lower the DoH by 2%, but would also divide the hydrogen mass flow rate by three and thus require a three times bigger scaling factor. Therefore, the target DoH of 0.22 was determined as a compromise between compact reactor design and LOHC utilization.

2.7.2. Reactor control

Four different states have been implemented for reactor control in general (see Fig. 4). A pressure of 0.3 MPa is assumed for each of the dehydrogenation modes, which is a permissible value for the fuel cell inlet pressure and allows decent conversion inside the dehydrogenation reactor. In addition, the heating medium temperature T_{HM} and the LOHC input mass flow $\dot{m}_{LOHC}$ are defined in each of the reactor control states.

Eco. This state is the default one and used in all scenarios. The priority in this state is to achieve high degrees of dehydrogenation. This means high temperature and low LOHC mass flow. High DoDHs are necessary to ensure a high real hydrogen capacity of the LOHC molecule as real hydrogen capacity decreases with decreasing DoDHs.

- T_{HM} = 330 °C

Fig. 4. Overview of the reactor control states.

- $\dot{m}_{LOHC} = 6\,\text{kg/h}$ (unscaled reactor)
- $DoDH = 0.78$
- $\dot{m}_{H2,reactor} = 0.30\,\text{kg/h}$ (unscaled reactor)

Boost. A boost mode can be activated for all PEMFC scenarios. In this mode, the LOHC mass flow will be increased and thus the released hydrogen mass flow increases, as the dehydrogenation of H18-DBT is dependent on the concentration of H18-DBT and accelerates with increasing concentration of H18-DBT. By increasing LOHC mass flow the residence time decreases resulting in lower DoDH and a lower hydrogen capacity of Hx-DBT in reality. Decreasing residence time or increasing mass flow leads to lower conversion of H18-DBT, resulting in a higher concentration of H18-DBT at the reactor outlet. There has been no fixed transition condition for the activation of this state implemented, instead the transition condition is a variable parameter, so that the optimization algorithm can test whether the usage of such a state makes sense with regard to the optimization goals.

- $T_{HM} = 330\,°\text{C}$
- $\dot{m}_{LOHC} = 20\,\text{kg/h}$ (unscaled reactor)
- $DoDH = 0.46$
- $\dot{m}_{H2,reactor} = 0.56\,\text{kg/h}$ (unscaled reactor)

Shutdown/off. For two PEMFC scenarios (self-sufficient and grid) also the "Shutdown" and the "Off" state are implemented. The "Shutdown" state becomes active, if either the target SOC has been reached (self-sufficient) or if the final destination has been reached (grid). In this state the heating medium temperature decreases exponentially and the LOHC mass flow is reduced linearly. When the LOHC mass flow is zero, the "Off" state is activated.

3. Powertrain optimization

The goal of this publication is the sizing of the powertrain system of a LOHC-based hydrogen train system. This is done for three different routes with different track characteristics. Furthermore, three different scenarios that differ in types of components and control strategy are investigated. The sizing, which includes also the parametrization of the control unit, involves a GA that minimizes three objective functions.

3.1. Investigated routes

Three different elevation profiles have been investigated (see ESI) based on real-world data in order to compare its influence on the powertrain sizing. Cuxhaven–Buxtehude (CB) is located far in the north of Germany and therefore offers a short, flat track. On this track Alstom's Coradia iLint has been in daily operation since 2022. The second track, Nürnberg–Leipzig (NL) in the south-eastern part of Germany, is a long track with steep ascent at the halfway point, whereas the third track, Radolfzell–Ulm, in the south-western part of Germany, is a short track with medium ascent at the beginning. Table 3 summarizes the information on the selected routes.

The number of one way trips is determined with the goal of having roughly the same overall distance at the end of the day. For all three routes artificial timetables have been created based on average speeds for different route lengths, which were obtained by a literature research on local train routes.

3.2. Investigated scenarios

In general, four different scenarios were implemented and evaluated.

Table 3
Route parameters.

	Cuxhaven–Buxtehude (CB)	Nürnberg–Leipzig (NL)	Radolfzell–Ulm (RU)
Distance one way	122 km	324 km	140 km
Total distance	976 km	972 km	980 km
Total time	14.3 h	13.2 h	13.6 h
Ascent	101 m	649 m	361 m
Height difference	5 m	−197 m	85 m

1. PEMFC (shutdown (sd), self-sufficient (ss)): No grid connection, battery recharge via PEMFC, shutdown of reactor and fuel cell at final destination overnight, when target SOC is reached
2. SOFC (24 h, self-sufficient (ss)): Grid connection at final train station, battery recharge via SOFC, feeding surplus electricity into the grid, no shutdown of reactor and fuel cell at final destination. Electricity is fed into the grid overnight to compensate missing PV power in the power grid.
3. PEMFC (shutdown (sd), recharge via grid (g)): Grid connection at final train station, battery recharge via grid, shutdown of reactor and fuel cell overnight when final destination has been reached
4. PEMFC (24 h, self-sufficient (ss)): Grid connection at final train station, battery recharge via PEM fuel cell, feeding surplus power into the grid, no shutdown of reactor and fuel cell at final destination. Electricity is fed into the grid overnight to compensate missing PV power in the power grid.

The scenarios mainly differ in the used fuel cell type, the control system and the operating time of the reactor and fuel cell. For the SOFC scenario, it is assumed that the exhaust gas of the fuel cell is sufficient to heat the thermal oil circuit, as already mentioned in Section 2.2. Hence, no released hydrogen has to be burned in an additional burner. However, since the thermal oil circuit's main volumetric component is the heat exchanger it is assumed that there are no volumetric and only 10% mass savings for the heating system in this scenario. Furthermore, potential savings for the gas purification unit, since SOFCs can also be operated at lower hydrogen purity, are not considered. In case of the two 24 h scenarios, the surplus electricity is fed into the local power grid and sold. For scenario 3 on the other hand the price for battery recharging via grid has to be paid. For all scenarios, one refueling process at the final train station is assumed, while for the scenario of battery charging via the grid, battery charging at the final train station is also assumed.

3.3. Optimization approach

For the dimensioning and parametrization of the powertrain a genetic algorithm based multi-objective optimization is applied. Three different fitness functions are to be minimized simultaneously by varying plant (x_p) and control variables (x_c) in a defined range.

$$\min\left(J_i\left(x_p, x_c, P_{train}\right) + X_{pen}\right) \tag{18}$$

Four plant and four control variables are implemented. The plant variables comprise the specific sizes of the main powertrain components (fuel cell, reactor, battery, LOHC tanks). The control variables are SOC values. Besides the initial SOC at the beginning of the simulation, this includes thresholds for activating and deactivating the boost mode and for switching off the reactor. However, not all control variables are

$$J_1 = LCOD = \frac{(CAPEX_{tot} + CAPEX_{exchange}) \cdot AF + OM_{tot} + OPEX_{LOHC,H2} + OPEX_{elec} - REV_{elec}}{s_{year}} \quad (19)$$

Box II.

relevant in some scenarios. For the 24 h scenarios the shutdown threshold is not used. Furthermore, no boost mode is implemented in the SOFC scenario, since it is assumed that the SOFC runs in steady-state mode due to its rather slow dynamic behavior.

Levelized costs of driving (LCOD). The LCOD function comprises overall capital expenditure $CAPEX_{tot}$, costs for exchange $CAPEX_{exchange}$, costs for operation and maintenance OM_{tot}, annuity factor AF, yearly operational costs for hydrogen stored in LOHC $OPEX_{LOHC,H2}$, for electricity $OPEX_{elec}$ and revenues for fed-in electricity REV_{elec}. $OPEX_{LOHC,H2}$ comprises the costs for LOHC-based hydrogen, which is based on data from Kwak et al. whereby the costs for dehydrogenation and combustion are neglected, as these take place on board the train and are therefore considered separately [52]. A distinction is made between the hydrogen production costs and the remaining costs, which include the hydrogenation process and transportation. The remaining costs are assumed to be constant and amount to 1.57 USD/kg. The hydrogen production costs, on the other hand, are determined as a function of the DoDH. With a DoDH of 95%, they amount to 4 USD/kg as in Kwak et al. $OPEX_{elec}$ are based on data of the German railroad infrastructure operator [53]. The total expenditure is related to the annual mileage s_{year} and thus given in EUR/km (see Eq. (19) in Box II).

By the usage of an annuity factor the one-time capital expenditure (CAPEX) is converted into an annual payment. The annualized overall capital expenditure ($ACAPEX_{tot}$) as well as the annualized costs for exchange ($ACAPEX_{exchange}$) are defined as follows.

$$ACAPEX_{tot} = CAPEX_{tot} \cdot AF \quad (20)$$

$$ACAPEX_{exchange} = CAPEX_{exchange} \cdot AF \quad (21)$$

Therefore, the depreciation period n and the weighted average cost of capital $WACC$ are required.

$$AF = \frac{(1 + WACC)^n \cdot WACC}{(1 + WACC)^n - 1} \quad (22)$$

$CAPEX_{tot}$ comprises the capital expenditure of all relevant powertrain components. Except for the reactor all CAPEX functions are scaled linearly. The reactor CAPEX is calculated via an exponential function with a scaling exponent of 0.6 (see Table 4).

$CAPEX_{exchange}$ covers the costs for replacing a certain component after exceeding its lifetime. They amount to 60% of the initial $CAPEX$ for PEMFC in accordance with Eypasch et al. numbers for PEM electrolysers [54] and to 100% for battery and LOHC pump.

Mass. The mass function comprises the masses of all relevant components of the powertrain, battery, fuel cell, LOHC tanks, H_2 tanks, reactor.

$$J_2 = m_{pt,tot} = m_{reactor} + m_{battery} + m_{fuelcell} + m_{LOHCtanks} + m_{H2tank} + m_{H2burner} \quad (23)$$

Volume. The volume function comprises the volumes of all relevant components of the powertrain.

$$J_3 = V_{pt,tot} = V_{reactor} + V_{battery} + V_{fuelcell} + V_{LOHCtanks} + V_{H2tank} + V_{H2burner} \quad (24)$$

For both, mass and volume function, battery, fuel cell, LOHC tanks and H_2 tanks are scaled linearly. LOHC and H_2 tanks are scaled by

increasing the number of tanks, while battery and fuel cell are scaled based on their rated power (W) and their energy content (kWh) respectively. The dehydrogenation reactor is scaled by increasing the number of tubes using a scaling factor by which the basic reactor (14 tubes) is multiplied. This approach is also applied for two heat exchangers, whose mass and volume are included in reactor mass and volume. See Table 5 for details on the scaling approach of the different components.

Penalties. Several technical constraints have been implemented.

- Battery SOC limits: $0.15 \leq x_{SOC} \leq 0.85$
- Battery final SOC value: $x_{SOC,init} \leq x_{SOC,final} \leq 1.02 \cdot x_{SOC,init}$
- Battery C-rate : $x_{c-rate} \leq 5$
- Fuel cell maximum part load ratio: $x_{FC,PLR} \leq 1$
- LOHC tank filling level limits: $0.1 \leq x_{tank,FL} \leq 1$

The SOC limit values of the battery are selected to minimize degradation. According to Woody et al. a SOC range of 0.2–0.8 should be aimed at [66]. Deviations of 0.05 were assumed to be acceptable, which leads to limits of 0.85 and 0.15. The SOC at the beginning of the day $x_{SOC,init}$ was a variable parameter of the optimization algorithm. The final SOC value at the end of the day should be at least the same size as $x_{SOC,init}$, but also not exceed 102% of $x_{SOC,init}$. A C-rate limit of 5 has been implemented according to available data on LTO batteries [60]. Since the fuel cell is controlled by the hydrogen output of the dehydrogenation reactor and no detailed control is implemented to minimize computational effort, a penalty for its PLR is implemented, which should not exceed 1. For the lower limit of the LOHC tank (H18-DBT) 0.1 is chosen to have a safety buffer. The upper limit concerns the tanks of the dehydrogenated LOHC (Hx-DBT). If one of these requirements is not met, a constant penalty of 500 (X_{pen}) will be added to the fitness function for each of the not met requirements, in order to "punish" this configuration to avoid a global minimum.

3.4. Selection of a configuration

In some scenarios and on some routes, the algorithm provides more than one configuration, and a corresponding control parameter set for the traction system. In this case, an exemplary configuration must be selected for a more detailed consideration of the cost structure. A selection procedure is proposed for this purpose. To select a configuration, the results of the multi-objective optimization are normalized for each route using the following equations, resulting in values between 0 and 1 for each objective.

$$J_{1,norm} = \frac{LCOD - \min(LCOD)}{\max(LCOD) - \min(LCOD)} \quad (25)$$

$$J_{2,norm} = \frac{m_{pt} - \min(m_{pt})}{\max(m_{pt}) - \min(m_{pt})} \quad (26)$$

$$J_{3,norm} = \frac{V_{pt} - \min(V_{pt})}{\max(V_{pt}) - \min(V_{pt})} \quad (27)$$

Finding the minimum sum of the normalized and weighted functions gives the components sizes for the scenario for each route. As can be seen from the weighting factors, the volume objective J_3 was prioritized slightly more than the others in order to consider the limited space aboard the train.

$$J_{final} = \min \left(0.3 \cdot J_{1,norm} + 0.3 \cdot J_{2,norm} + 0.4 \cdot J_{3,norm} \right) \quad (28)$$

Table 4
Economic parameters.

Component	Costs	Unit	Reference	OM	Reference	Lifetime	Reference
PEMFC	76	USD/kW	[55]	6%	[56]	15,000 h	[57]
SOFC	2170	EUR/kW$_{el}$	[58]	6%	[56]	100,000 h	[58]
H$_2$ tank	250	EUR/kg$_{H2}$	[59]	2%	[59]	20 a	[59]
Battery	220	USD/kWh	[60]	3%	[29]	10 a	[60]
H$_2$ burner	$0.08696 \cdot P_{th,H2} + 1.278 \cdot 10^5$	EUR/kW$_{H2}$	Internal data	2%	Assumption	20 a	Assumption
LOHC tanks	4058	EUR/m^3	[48]	2%	[59]	20 a	
LOHC pump	500	EUR/t$_{H2,day}$	[59]	3%	[59]	10 a	[59]
LOHC reactor	$30 \cdot 10^6 \cdot \left(\frac{m_{H2,day}}{300\,t} \right)^{0.6}$	EUR/kg$_{H2,day}$	[61]	3%	[59]	20 a	[59]

Parameter	Value	Unit	Reference
WACC	6%	–	Assumption
Depreciation period	20	a	Assumption
Days of train usage per week	6	–	Assumption
Weeks of train usage per year	49	–	Assumption
Hydrogen costs (LOHC)	$(4 \cdot \frac{DoDH}{0.95} + 1,57)$	USD/kg	[52]
Electricity cost	0.068 (if usage time < 2500 h)	EUR/kWh	[53]
	0.017 (if usage time ≥ 2500 h)		
Electricity remuneration	0.0273	EUR/kWh	[53]
Currency conversion	0.94	EUR/USD	[62]

Table 5
Scaling parameters of powertrain components.

Component	Mass			Volume		
	Scaling factor	Unit	Reference	Scaling factor	Unit	Reference
PEMFC	3.3	kg/kW	[63]	0.4	m^3/MW	[64]
SOFC	11.0	kg/kW	[65]	5.0	m^3/MW	[65]
Battery	10.1	kg/kWh	[60]	4.6	m^3/MWh	[60]
LOHC tank	214	kg/tank	[48]	1.6	m^3/tank	[48]
H$_2$ tank	133	kg/tank	Calculated	74.5	l/tank	Calculated

In the following, the results of the first scenario PEMFC (sd, ss) are examined in more detail, as PEMFCs already have a good technology readiness level (TRL) and complete self-sufficiency could be more relevant for rapid implementation. Of the three routes, the configuration of route CB is chosen as it has a less demanding elevation profile than the other routes and could therefore represent a good initial application scenario. On this route, only one parameter combination is obtained through the optimization process.

4. Results and discussion

The results are divided into two parts. First, the results of the powertrain optimization are presented, covering the different scenarios and routes investigated. Secondly, more detailed results for one single scenario are discussed. As already mentioned in Section 2, the power profile optimization is not discussed in more detail. However, the average specific energy requirement will be given in order to evaluate the methodological approach and better classify the results. These values were between 3.02 and 3.41 kWh/km for the three route profiles. A German reference gives the electrical energy demand of 4.05 kWh/km for a slightly lighter train with a similar total daily distance, but more frequent stops and acceleration processes, which are the main energy consumers [67].

4.1. Powertrain optimization

As described in Section 2.7.2 the transition conditions for entering and leaving the boost mode for all three PEMFC scenarios were parameters of the optimization algorithm. The conclusion here is that the GA did use this mode four times in nine possible cases (three different routes and three different PEMFC scenarios). Boost mode is used in scenario PEMFC (sd, ss) on route NL, in scenario PEMFC (24, ss) on route CB and NL, and in some configurations for route RU. The ambiguity of the results shows that it is difficult to make generalized statements about the boost mode. However, it can be stated that under

the assumed constraints, a boost mode makes sense with regard to the fitness functions LCOD, mass and volume, especially in PEMFC 24 hour scenarios. The constraints for reactor control primarily include the scaling functions of the components as well as the time required for a change of operating point. The reason for the use in long scenarios is presumably that a lot of volume is already taken up by the LOHC tanks due to the assumed refueling strategy of one refueling process per day. This can be reduced by using a boost mode and outweighs the additional weight and the additional price. However, a new reactor control, e.g. by varying the pressure inside the reactor and hence also the reaction kinetics, would enable a more dynamic operation of the reactor and the fuel cell. In addition, a new heating or reactor concept itself could allow a better heat transfer into the catalytic bed, which could also lower the time to change the operating point [20,68]. These adjustments could improve a boost mode in general on all routes and might make it more attractive.

The results of the optimized sizing are shown via bar plots. The length of the bars is defined by the configuration selection approach, if more than one solution is given by the optimization algorithm. Additional small black bars indicate the minimum and maximum values if further solutions exist. Fig. 5 shows the results for the LCOD parameter for each scenario on each route. The detailed shares of those costs for one scenario are discussed in Section 4.2. A comparison of the selected configurations of the different scenarios shows a general trend for all three routes. The PEMFC 24 h scenario (3.39–3.72 EUR/km) and the SOFC scenario (2.93–3.28 EUR/km) are the most expensive scenarios. This is because of the longer operating hours of the reactor and fuel cell systems and thus the higher demand of LOHC, while the distance traveled remains unchanged. Even the feeding of surplus electricity into the grid cannot compensate for this.

When comparing the two 24 h scenarios, the SOFC scenario is cheaper, although the SOFC itself causes higher investment and exchange costs despite its significantly lower rated power and longer lifetime, and although the usage of the boost mode in the PEMFC scenario enables smaller and cheaper reactors. However, these higher costs are compensated for by the fact that in the SOFC scenario less
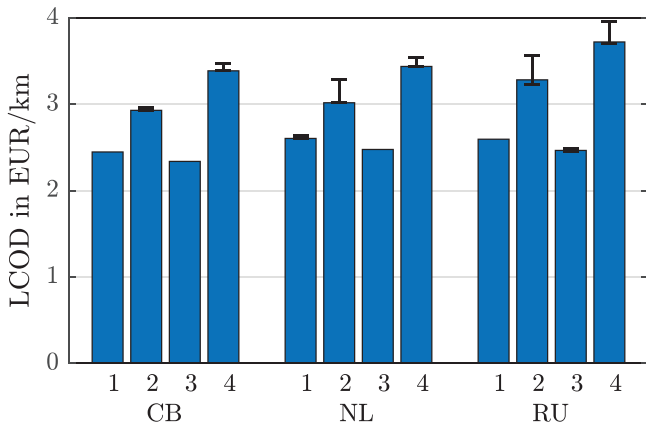
Fig. 5. Powertrain LCOD of different scenarios and routes (Numbers correspond to the scenarios).

Fig. 6. Powertrain masses of different scenarios and routes (Numbers correspond to the scenarios analyzed).

LOHC tanks are sufficient, since no extra hydrogen burner has to be supplied with hydrogen by the dehydrogenation reactor.

In contrast, the two scenarios in which the fuel cell is shut down either when the target SOC has been reached or when the train has reached its final destination, are significantly cheaper than the 24 h self-sufficient scenarios. The costs for start-up/ heating of the dehydrogenation unit are roughly estimated by calculating the required amount of energy for heating up the (steel) mass of the LOHC reactor $m_{steel,reactor}$ from ambient temperature via the following equation.

$$Q = m_{steel,reactor} \cdot c_{p,steel} \cdot \Delta T \tag{29}$$

Additional costs for a heat up via hydrogen burning between 0.03 and 0.04 EUR/km and via electrical heating of up to 0.01 EUR/km, depending on the reactor size, would have to be considered. These findings apply to the current economic framework conditions. In the future of renewable energies, other framework conditions, e.g. no longer a constant electricity price, could lead to different results and might make 24 h scenarios economically more competitive. Comparing the two cheapest scenarios among each other under current conditions shows minor economic advantages for the grid scenario (2.34–2.48 EUR/km vs. 2.45–2.60 EUR/km, as recharging the battery using hydrogen stored in LOHC is more expensive than using electricity directly via the grid. In other words, the additional costs for electricity are small compared to the savings in LOHC material.

The results described above apply if the costs are related to annual mileage. If they are related to the operating hours of the fuel cell/reactor, the two 24 h scenario offer the cheapest powertrain system, with the SOFC scenario being cheaper than the PEMFC scenario. In this case, the additional costs due to the higher LOHC demand are compensated for by the longer operating time. This means that the economic evaluation of this new operating concept with continuous drive train operation depends on the reference value used.

For the second objective function the following results are obtained. In general, the main contributors to the overall powertrain mass for the PEMFC scenarios are LOHC tanks (incl. LOHC material), reactor and battery. For the SOFC scenario the SOFC is also relevant for the overall mass because of its comparatively high weight. When comparing the four scenarios on the three routes, a similar trend for the mass parameter as with LCOD becomes clear. This can be seen in Fig. 6, where the overall powertrain masses of the selected configurations as well as the respective shares of the different powertrain components are displayed. The two 24 h self-sufficient scenarios (PEMFC (24, ss) and SOFC (24, ss)) are the heaviest on routes CB and RU, as more LOHC material is required for the all-day operation of the LOHC reactor and fuel cell than for the shutdown scenarios. The higher weight for the first scenario on route NL is due to the usage of the boost mode and
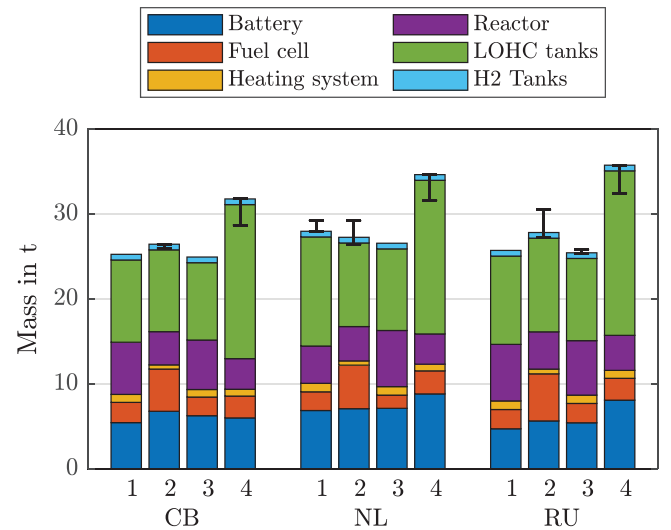
the resulting higher LOHC demand. Although the SOFC scenario uses a heavier fuel cell than the PEMFC (24, ss) scenario (specifically and absolutely) on all routes, the PEMFC (24, ss) scenario (31.8–35.7 t) is generally heavier than the SOFC scenario (26.4–27.8 t). This is due to the lower demand for hydrogen and thus LOHC material as well as a lighter heating system, as the SOFC exhaust gas is used for the reactor heating and no boost mode is used. These advantages compensate for the heavier fuel cell and reactor and, in the case of the CB route, the larger and therefore heavier battery.

When comparing the two PEMFC scenarios with shutdown, the PEMFC grid scenario is slightly lighter than the PEMFC self-sufficient scenario on all routes. A slightly smaller reactor and thus less LOHC tanks are used for the grid shutdown scenario comparing scenarios without boost mode usage. In the case of route NL, the PEMFC self-sufficient scenario has a lighter reactor due to the use of the boost mode. However, the additional demand of LOHC compensates for this advantage. This means that in all cases the larger battery of the PEMFC grid scenario, which leads to a slightly higher demand for recharging energy, can be compensated for.

Generally, different approaches exist for weight savings, which mainly address the LOHC system. Reducing the conservative target of 10% of LOHC tank level at the end of the journey could allow weight savings. In addition, the possibility of refueling the LOHC at the train station throughout the day would also enable a significant weight reduction. In this way, the LOHC tank size and the powertrain mass — not the LOHC demand — could be reduced. This applies to all scenarios. However, the weight saving potential are bigger for the self-sufficient scenarios, as the refueling process is assumed to take place after recharging the battery (PEMFC, sd, ss) or at the end of the day (24 h scenarios), whereas the battery recharging via grid starts directly when arriving at the final train station. An increased DoDH, which means better utilization of the stored hydrogen, would also allow smaller LOHC tanks and thus reduce the LOHC (tank) mass. As already described at the beginning of Section 4.1 new approaches for the reactor system could enable more power dense and thus lighter reactors. This also includes the approach of direct usage of the exhaust gas of the SOFC for the dehydrogenation of the LOHC, which makes the thermal oil system redundant.

With regard to the total volume of the powertrain, the SOFC scenario indicates advantages (44.8–49.9 m^3) not only over the PEMFC (24, ss) scenario (59.8–67.7 m^3), but also compared to the two shutdown scenarios. This can be seen in Fig. 7, which shows not only
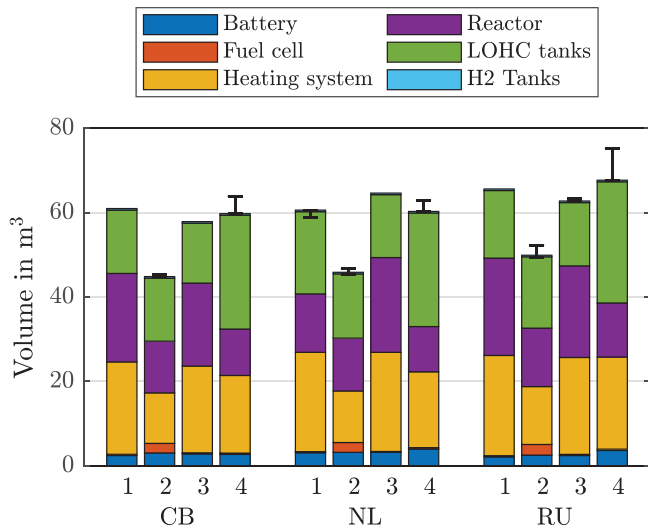
Fig. 7. Powertrain volumes of different scenarios and routes (Numbers correspond to the scenarios).

Table 6

Exemplary configuration and control parameters based on scenario 1 and route CB.

Component	Size
Rated power of PEMFC	722 kW
Scaling factor of reactor	82
Hydrogen release rate of scaled reactor (Eco)	24.6 kg/h ≈ 820 kW_{LHV-H2}
Number of tubes of scaled reactor	1148 (82 · 14 tubes)
Catalyst mass of scaled reactor	335 kg (82 · 4.08 kg)
Battery capacity	537 kWh
Number of LOHC tanks (incl. one empty tank)	9.4
SOC_{init}	0.63
$SOC_{shut-down,enter}$	0.44
$SOC_{boost,enter}$	0.17
$SOC_{boost,leave}$	0.66

the total volume but also the respective shares of the powertrain components. The advantages of the SOFC scenario compared to the two PEMFC shut-down scenarios are mainly based on the smaller heating system, which has a high share of the overall volume. This also compensates for the larger volumetric size of the SOFC and even the larger number of LOHC tanks required for 24 h operation. Compared to the PEMFC 24 h scenario, the smaller number of LOHC tanks and the smaller heating system are decisive for the smaller volume demand. On route NL, the usage of the boost mode with a smaller reactor system enables the second smallest volume for the PEMFC (sd, ss) scenario, whereas on the other routes the PEMFC (sd, g) scenario has the second smallest volume demand due to less LOHC tanks compared to the PEMFC (24, ss) scenario and due to a smaller reactor compared to the PEMFC (sd, ss) scenario.

Further volume reduction potential still exists for the SOFC scenario, as it was conservatively assumed that a thermal oil cycle is needed, which might be redundant by a direct exhaust gas heating of the dehydrogenation reactor.

In general, the greatest potential for volumetric optimization lies in the energy supply for the dehydrogenation reactor and the reactor itself. New approaches for hydrogen burners, e.g. catalytic burners integrated into the reactor, offer huge volumetric savings. The direct usage of fuel cell exhaust gas in the reactor is another promising approach [17] but has not yet been demonstrated.

Finally, the results described above are briefly analyzed below. Din et al. did an analysis for the retrofitting of a diesel-based British rail class 150 to a hydrogen–hybrid powertrain. Their system design resulted in a total mass for the fuel cell, battery and 35 MPa tanks of 4.5% of the total train mass. In the best case (PEMFC, sd, g), a share of approx. 20.9% can be achieved for the LOHC train with the assumptions made in this publication. As described above, optimization potential lies in the reduction of the LOHC (tank) mass and direct usage of fuel cell exhaust gas as well as a more dynamic and smaller reactor system, which would possibly also enable smaller and lighter batteries. In terms of volume, Din et al. calculated a required total volume for fuel cell, battery and H_2 tanks of 51.5 m^3 [69]. The LOHC train can reach a comparable and even better value, with 44.9 m^3 as minimum. Overall, the results described also offer optimization potential, because conservative assumptions are made that are based on existing and implemented stationary projects. Furthermore, a LOHC-based hydrogen train can save investment costs in terms of refueling infrastructure, as the existing fossil fuel-based refueling infrastructure can be (re)used.

According to Caponi et al. hydrogen refueling stations (HRS) on a delivery basis would require investment costs related to the daily capacity of 4000 EUR/kg/day to 6000 EUR/kg/day [70]. For a HRS with a capacity of 1600 kg/day, as introduced by Linde for Alstom's hydrogen train fleet in northern Germany [71], investment costs of 6.4 to 9.6 million EUR would result. Besides that, safety advantages of the LOHC train — less elemental hydrogen is handled aboard the train — are also worth mentioning due to high safety requirements in the rail sector.

4.2. Configuration scenario 1

Table 6 shows the resulting configuration of a LOHC-based hydrogen train system for scenario 1 on route CB. Detailed investigations show that the relatively high rated power for the fuel cell is acceptable, as it is operated at a good efficiency and has consequently a lower hydrogen demand, which then enables a smaller reactor. This is relevant as LOHC demand is the most important component concerning LCOD, which will be discussed later. Furthermore, the assumed dynamics of the reactor and thus the fuel cell are rather low, as a change of the operating point takes a relatively long time and therefore the dynamics requirements are mainly covered by the battery. As discussed at the beginning of Section 4.1, a more dynamic operation of the reactor might be possible, which offers optimization potential concerning the component sizing. However, boost mode operation currently requires more thermal power, which means a bigger hydrogen burner is necessary, as the sizing is based on the maximum thermal output. New space-saving approaches for the energy supply are therefore also needed. At the same time, it must be taken into account that information on several technical and economic parameters would be required for a detailed comparison with existing train models. This involves train mass, recuperation and acceleration behavior as well as cost functions of components, hydrogen prices and costs for hydrogen refueling infrastructure among others. The optimization algorithm sets the transition condition for the transition to boost mode to 0.17, but since the SOC does not fall below this threshold, boost mode is not used. The initial state of charge is set to 0.66.

For this configuration an economic analysis was done, which gives the distribution of the levelized costs of driving (LCOD) and breaks down the capital expenditure ($CAPEX_{tot}$) (see Fig. 8). The OPEX accounts for the largest share of the LCOD, followed by $ACAPEX_{tot}$, costs for operation and maintenance and exchange costs for components. The distribution of the capital expenditure shows that the biggest share (61%) is covered by the reactor system. However, there are still possibilities for cost reduction for this component, as with the currently assumed DoDH of roughly 78% the general potential of LOHC technology has not yet been fully exploited. There are reports that even higher DoDHs can be achieved with this reactor technology [23]. This would allow savings in LOHC demand while maintaining the same hydrogen release. Furthermore, the selected cost function is based on a classical reactor type. New approaches might offer cost reduction potential. For example, by inverting the catalyst chamber and the
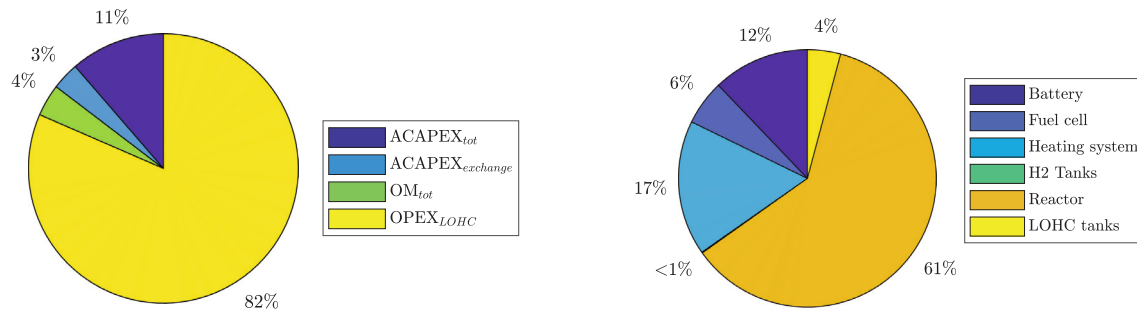
Fig. 8. Distribution of powertrain LCOD (left) and powertrain CAPEX$_{tot}$ (right) for scenario PEMFC (sd, ss) on route CB.

thermal oil chamber, the power density can be increased, which enables smaller reactors [20,68]. After LOHC-related components (reactor, H$_2$ burner) the battery costs have the second highest share of the CAPEX$_{tot}$. However, at only 12%, the cost reduction potential is comparatively small. This also applies to the rest of the powertrain components, namely fuel cell, LOHC tanks and hydrogen tanks.

5. Conclusion and outlook

In this publication, the first techno-economic analysis of a LOHC-based hydrogen train was done by dynamic simulation and optimization methods. For this purpose, the models of the relevant components of the powertrain system were implemented and combined to an overall powertrain system. Four different scenarios were investigated. In three scenarios, the released hydrogen was converted into electricity in a PEMFC and in one scenario, hydrogen was converted in a SOFC. The latter and one PEMFC scenario include a reactor and fuel cell operation for 24 h, while the other two PEMFC scenarios are based on a daily shutdown of the reactor and fuel cell. For the SOFC scenario, a daily shutdown is not feasible due to limited SOFC dynamics. In the shutdown scenarios, the battery is either recharged via fuel cell or via electrical grid. Besides those four scenarios, three different artificial timetables for real world elevation profiles were used for the simulation and optimization of a day trip of the train system. Based on the track profile and the artificial timetables, a train speed profile was determined as a basis for all design configurations of the LOHC-based train. The LOHC-based train consists of a LOHC tank, a hydrogen release unit, a heating unit, a fuel cell and a battery for smoothing the power profile. For each scenario and configuration, the individual components were sized using a multi-objective genetic algorithm to obtain the best overall train design. The levelized costs of driving, the system volume and mass are used as optimization parameters. The LCOD range from 2.34 to 3.72 EUR/km, the mass of the total system is between 24.9 to 35.7 t and the volume between 44.8 to 67.7 m^3. The evaluated total system volume is smaller than the volume for a comparable hydrogen fueled train supplied with compressed hydrogen [69]. LCOD was not assessed in the study by Din et al. However, Runge et al. assessed the mobility costs for heavy-duty vehicles supplied with hydrogen or derivatives produced at excellent locations. In their scenario, hydrogen was transported as H18-DBT and released at the refueling station and then dispensed into the vehicle as compressed hydrogen. If the LOHC can be filled directly into the vehicle and the hydrogen is released on board, the costs for the refueling station are eliminated, resulting in the lowest mobility costs for LOHC-bound hydrogen compared to the other vectors. Based on the study by Runge et al. the logistic costs for LOHC-bound hydrogen should be lower for a train fueled with LOHC bound hydrogen compared to other vectors, when all hydrogen supply costs are considered [30].

A scenario was selected and analyzed to evaluate the key components that need to be improved in order to reduce the overall volume and LCOD. The LCOD is dominated by the costs of hydrogen supply, which are predominantly dependent on the achieved DoDH.

Increasing the DoDH can significantly reduce the LCOD. Currently, optimized catalysts or better LOHC systems are developed to improve the performance in the hydrogen release unit and thus enable higher LOHC utilization and reducing LCOD [72,73]. The volume of the total system is dominated by the reactor and heating system size. The reactor volume can be decreased by using the recently reported inverted fixed-bed reactor design [68]. Additionally, a reactor which combines an exothermal reaction (hydrogen combustion or partial LOHC oxidation) in one reactor compartment and the endothermal dehydrogenation in the other compartment can eliminate the need of a separate heating system and significantly reduce the total system volume [74]. Direct utilization of the SOFC exhaust gas would also be a viable option to eliminate the heating system for the SOFC scenario and thus reduce the total system volume.

Overall, the developed model allows the design of a power supply system for vehicles based on LOHC technology. Other promising vehicles that could be supplied with LOHC based power might be ships, agricultural machinery or freight trains. The power profile needs to be adapted for the desired scenario. However, the proposed models are independent on size and can also be used for different power outputs. Furthermore, the use of independent models for each main unit allows the addition of new units, the replacement of existing units, e.g. the replacement of the fuel cell with an internal combustion engine, or the updating of units if a significant improvement is achieved.

CRediT authorship contribution statement

Christoph Regele: Writing – original draft, Visualization, Validation, Software, Methodology, Investigation, Formal analysis, Data curation. **Felix Gackstatter:** Writing – review & editing, Investigation. **Florian Ortner:** Writing – review & editing, Investigation. **Patrick Preuster:** Writing – review & editing, Supervision, Project administration, Conceptualization. **Michael Geißelbrecht:** Writing – review & editing, Supervision, Resources, Project administration, Conceptualization.

Declaration of competing interest

The authors declare the following financial interests/personal relationships which may be considered as potential competing interests: Michael Geisselbrecht reports financial support was provided by Bavarian Ministry of Economic Affairs, Regional Development and Energy. If there are other authors, they declare that they have no known competing financial interests or personal relationships that could have appeared to influence the work reported in this paper.

Acknowledgments

Appendix A. Supplementary data

Supplementary material related to this article can be found online at https://doi.org/10.1016/j.enconman.2025.120234.

Data availability

Data will be made available on request.

References

[1] Hannah Ritchie, Max Roser, Pablo Rosado. CO_2 and greenhouse gas emissions. Our World Data 2020. URL https://ourworldindata.org/emissions-by-sector.

[2] Zheng S, Krol A. Public transportation. 2023, URL https://climate.mit.edu/explainers/public-transportation,

[3] International Energy Acency. GHG intensity of passenger transport modes, 2019. 2020, URL https://www.iea.org/data-and-statistics/charts/ghg-intensity-of-passenger-transport-modes-2019.

[4] Railway Pro. Worldwide rail electrification remains at high volume. 2021, URL https://www.railwaypro.com/wp/worldwide-rail-electrification-remains-at-high-volume/.

[5] Kim M-K, Park D, Kim M, Heo J, Park S, Chong H. A study on characteristic emission factors of exhaust gas from diesel locomotives. Int J Environ Res Public Heal 2020;17(11). http://dx.doi.org/10.3390/ijerph17113788.

[6] Geerts E. Will battery or hydrogen trains be the future? The vision of siemens mobility. 2023, URL https://www.railtech.com/rolling-stock/2023/05/04/will-battery-or-hydrogen-trains-be-the-future-the-vision-of-siemens-mobility/,

[7] Sun Y, Anwar M, Hassan NMS, Spiryagin M, Cole C. A review of hydrogen technologies and engineering solutions for railway vehicle design and operations. Railw Eng Sci 2021;29(3):212–32. http://dx.doi.org/10.1007/s40534-021-00257-8.

[8] Böhm M, Del Fernández Rey A, Pagenkopf J, Varela M, Herwartz-Polster S, Nieto Calderón B. Review and comparison of worldwide hydrogen activities in the rail sector with special focus on on-board storage and refueling technologies. Int J Hydrog Energy 2022;47(89):38003–17. http://dx.doi.org/10.1016/j.ijhydene.2022.08.279.

[9] Xu Z, Zhao N, Hillmansen S, Roberts C, Yan Y. Techno-economic analysis of hydrogen storage technologies for railway engineering: A review. Energies 2022;15(17):6467. http://dx.doi.org/10.3390/en15176467.

[10] Lee J-S, Cherif A, Yoon H-J, Seo S-K, Bae J-E, Shin H-J, et al. Large-scale overseas transportation of hydrogen: Comparative techno-economic and environmental investigation. Renew Sustain Energy Rev 2022;165:112556. http://dx.doi.org/10.1016/j.rser.2022.112556.

[11] Preuster P, Papp C, Wasserscheid P. Liquid organic hydrogen carriers (LOHCs): Toward a hydrogen-free hydrogen economy. Acc Chem Res 2017;50(1):74–85. http://dx.doi.org/10.1021/acs.accounts.6b00474.

[12] Niermann M, Drünert S, Kaltschmitt M, Bonhoff K. Liquid organic hydrogen carriers (LOHCs) – techno-economic analysis of LOHCs in a defined process chain. Energy Environ Sci 2019;12(1):290–307. http://dx.doi.org/10.1039/C8EE02700E.

[13] Zakgeym D, Hofmann JD, Maurer LA, Auer F, Müller K, Wolf M, et al. Better through oxygen functionality? The benzophenone/dicyclohexylmethanol LOHC-system. Sustain Energy & Fuels 2023;7(5):1213–22. http://dx.doi.org/10.1039/D2SE01750D.

[14] Dürr S, Zilm S, Geißelbrecht M, Müller K, Preuster P, Bösmann A, et al. Experimental determination of the hydrogenation/dehydrogenation — Equilibrium of the LOHC system H0/H18-dibenzyltoluene. Int J Hydrog Energy 2021;46(64):32583–94. http://dx.doi.org/10.1016/j.ijhydene.2021.07.119.

[15] Brückner N, Obesser K, Bösmann A, Teichmann D, Arlt W, Dungs J, et al. Evaluation of industrially applied heat-transfer fluids as liquid organic hydrogen carrier systems. ChemSusChem 2014;7(1):229–35. http://dx.doi.org/10.1002/cssc.201300426.

[16] Müller K, Thiele S, Wasserscheid P. Evaluations of concepts for the integration of fuel cells in liquid organic hydrogen carrier systems. Energy Fuels 2019;33(10):10324–30. http://dx.doi.org/10.1021/acs.energyfuels.9b01939.

[17] Preuster P, Fang Q, Peters R, Deja R, van Nguyen N, Blum L, et al. Solid oxide fuel cell operating on liquid organic hydrogen carrier-based hydrogen — making full use of heat integration potentials. Int J Hydrog Energy 2018;43(3):1758–68. http://dx.doi.org/10.1016/j.ijhydene.2017.11.054.

[18] Dennis J, Bexten T, Petersen N, Wirsum M, Preuster P. Model-based analysis of a liquid organic hydrogen carrier (LOHC) system for the operation of a hydrogen-fired gas turbine. J Eng Gas Turbines Power 2021;143(3). http://dx.doi.org/10.1115/1.4048596.

[19] Biswas S, Moreno Sader K, Green WH. Perspective on decarbonizing long-haul trucks using onboard dehydrogenation of liquid organic hydrogen carriers. Energy Fuels 2023;37(22):17003–12. http://dx.doi.org/10.1021/acs.energyfuels.3c01919.

[20] Bollmann J, Mitländer K, Beck D, Schühle P, Bauer F, Zigan L, et al. Burner-heated dehydrogenation of a liquid organic hydrogen carrier (LOHC) system. Int J Hydrog Energy 2023. http://dx.doi.org/10.1016/j.ijhydene.2023.04.062.

[21] Fikrt A, Brehmer R, Milella V-O, Müller K, Bösmann A, Preuster P, et al. Dynamic power supply by hydrogen bound to a liquid organic hydrogen carrier. Appl Energy 2017;194:1–8. http://dx.doi.org/10.1016/j.apenergy.2017.02.070.

[22] Willer M, Preuster P, Malgaretti P, Harting J, Wasserscheid P. Heat transfer to a catalytic multiphase dehydrogenation reactor. Int J Hydrog Energy 2024;80:1011–20. http://dx.doi.org/10.1016/j.ijhydene.2024.07.073.

[23] Willer M, Preuster P, Geißelbrecht M, Wasserscheid P. Continuous dehydrogenation of perhydro benzyltoluene and perhydro dibenzyltoluene in a packed bed vertical tubular reactor — The role of LOHC evaporation. Int J Hydrog Energy 2024;57:1513–23. http://dx.doi.org/10.1016/j.ijhydene.2024.01.031.

[24] Wunsch A, Mohr M, Pfeifer P. Intensified LOHC-dehydrogenation using multi-stage microstructures and Pd-based membranes. Membranes 2018;8(4). http://dx.doi.org/10.3390/membranes8040112.

[25] Solymosi T, Auer F, Dürr S, Preuster P, Wasserscheid P. Catalytically activated stainless steel plates for the dehydrogenation of perhydro dibenzyltoluene. Int J Hydrog Energy 2021;46(70):34797–806. http://dx.doi.org/10.1016/j.ijhydene.2021.08.040.

[26] Badakhsh A, Song D, Moon S, Jeong H, Sohn H, Woo Nam S, et al. CO_X-free LOHC dehydrogenation in a heatpipe reformer highly integrated with a hydrogen burner. Chem Eng J 2022;449:137679. http://dx.doi.org/10.1016/j.cej.2022.137679.

[27] Geiling J, Steinberger M, Ortner F, Seyfried R, Nuß A, Uhrig F, et al. Combined dynamic operation of PEM fuel cell and continuous dehydrogenation of perhydro-dibenzyltoluene. Int J Hydrog Energy 2021;46(72):35662–77. http://dx.doi.org/10.1016/j.ijhydene.2021.08.034.

[28] Ahluwalia RK, Hua TQ, Peng JK. On-board and off-board performance of hydrogen storage options for light-duty vehicles. Int J Hydrog Energy 2012;37(3):2891–910. http://dx.doi.org/10.1016/j.ijhydene.2011.05.040.

[29] Runge P, Sölch C, Albert J, Wasserscheid P, Zöttl G, Grimm V. Economic comparison of electric fuels produced at excellent locations for renewable energies: A scenario for 2035. SSRN Electron J 2020. http://dx.doi.org/10.2139/ssrn.3623514.

[30] Runge P, Sölch C, Albert J, Wasserscheid P, Zöttl G, Grimm V. Economic comparison of electric fuels for heavy duty mobility produced at excellent global sites — A 2035 scenario. Appl Energy 2023;347:121379. http://dx.doi.org/10.1016/j.apenergy.2023.121379.

[31] Meegahawatte D, Hillmansen S, Roberts C, Falco M, McGordon A, Jennings P. Analysis of a fuel cell hybrid commuter railway vehicle. J Power Sources 2010;195(23):7829–37. http://dx.doi.org/10.1016/j.jpowsour.2010.02.025.

[32] Hoffrichter A, Roberts C, Hillmansen S. Conceptual propulsion system design for a hydrogen-powered regional train. IET Electr Syst Transp 2016;6(2):56–66. http://dx.doi.org/10.1049/iet-est.2014.0049.

[33] Fragiacomo P, Piraino F. Fuel cell hybrid powertrains for use in Southern Italian railways. Int J Hydrog Energy 2019;44(51):27930–46. http://dx.doi.org/10.1016/j.ijhydene.2019.09.005.

[34] Zenith F, Isaac R, Hoffrichter A, Thomassen MS, Møller-Holst S. Techno-economic analysis of freight railway electrification by overhead line, hydrogen and batteries: Case studies in Norway and USA. Proc Inst Mech Eng Part F: J Rail Rapid Transit 2020;234(7):791–802. http://dx.doi.org/10.1177/0954409719867495.

[35] Garcia P, Fernández LM, Garcia CA, Jurado F. Comparative study of PEM fuel cell models for integration in propulsion systems of urban public transport. Fuel Cells 2010;10(6):1024–39. http://dx.doi.org/10.1002/fuce.201000002.

[36] Silvas E, Hofman T, Murgovski N, Etman P, Steinbuch M. Review of optimization strategies for system-level design in hybrid electric vehicles. IEEE Trans Veh Technol 2016;1. http://dx.doi.org/10.1109/TVT.2016.2547897.

[37] Sarma U, Ganguly S. Determination of the component sizing for the PEM fuel cell-battery hybrid energy system for locomotive application using particle swarm optimization. J Energy Storage 2018;19:247–59. http://dx.doi.org/10.1016/j.est.2018.08.008.

[38] Filipović Ž. Elektrische bahnen. Berlin, Heidelberg: Springer Berlin Heidelberg; 2015, http://dx.doi.org/10.1007/978-3-642-45227-7.

[39] Bombardier talent 2. URL https://de.wikipedia.org/wiki/Bombardier_Talent_2.

[40] Siemens mireo. URL https://en.wikipedia.org/wiki/Siemens_Mireo.

[41] Siemens Mobility GmbH. Mireo Plus B, Mireo Plus H. URL https://assets.new.siemens.com/siemens/assets/api/uuid:0a451202-2be4-485d-a736-974d74263e63/siemens-mobility-mireo-plus-b-mireo-plus-h-en.pdf.

[42] Herwartz S, Pagenkopf J, Streuling C. Sector coupling potential of wind-based hydrogen production and fuel cell train operation in regional rail transport in Berlin and brandenburg. Int J Hydrog Energy 2021;46(57):29597–615. http://dx.doi.org/10.1016/j.ijhydene.2020.11.242.

[43] Barbir F. PEM fuel cells: Theory and practice. 2nd ed.. Amsterdam and Boston: Elsevier/Academic Press; 2013, http://dx.doi.org/10.1016/B978-0-12-416012-5.00011-6.

[44] Lohse-Busch H, Duoba M, Stutenberg K, Iliev Simeon, Kern M, Richards B, et al. Technology assessment of a fuel cell vehicle: 2017 toyota mirai. 2018, URL https://publications.anl.gov/anlpubs/2018/06/144774.pdf,

[45] Hu X, Deng X, Wang F, Deng Z, Lin X, Teodorescu R, et al. A review of second-life lithium-ion batteries for stationary energy storage applications. Proc IEEE 2022;110(6):735–53. http://dx.doi.org/10.1109/JPROC.2022.3175614.

[46] Zhou D, Al-Durra A, Gao F, Ravey A, Matraji I, Godoy Simões M. Online energy management strategy of fuel cell hybrid electric vehicles based on data fusion approach. J Power Sources 2017;366:278–91. http://dx.doi.org/10.1016/j.jpowsour.2017.08.107.

[47] Aslam R, Khan MH, Ishaq M, Müller K. Thermophysical studies of dibenzyltoluene and its partially and fully hydrogenated derivatives. J Chem Eng Data 2018;63(12):4580–7. http://dx.doi.org/10.1021/acs.jced.8b00652.

[48] DENIOS SE. IBC-container TA aus Edelstahl. URL https://www.denios.de/ibc-container-ta-aus-edelstahl-rechteckbehaelter-137266/137266.

[49] Peters R, Deja R, Fang Q, van Nguyen N, Preuster P, Blum L, et al. A solid oxide fuel cell operating on liquid organic hydrogen carrier-based hydrogen — A kinetic model of the hydrogen release unit and system performance. Int J Hydrog Energy 2019;44(26):13794–806. http://dx.doi.org/10.1016/j.ijhydene.2019.03.220.

[50] Geißelbrecht M, Benker R, Seidel A, Preuster P. Modeling of the continuous dehydrogenation of perhydro–dibenzyltoluene in a cuboid reactor. Energy Technol 2024. http://dx.doi.org/10.1002/ente.202300813.

[51] Springer-Verlag GmbH. VDI-Wärmeatlas. Berlin, Heidelberg: Springer Berlin Heidelberg; 2013, http://dx.doi.org/10.1007/978-3-642-19981-3.

[52] Kwak Y, Kirk J, Moon S, Ohm T, Lee Y-J, Jang M, et al. Hydrogen production from homocyclic liquid organic hydrogen carriers (LOHCs): Benchmarking studies and energy-economic analyses. Energy Convers Manage 2021;239:114124. http://dx.doi.org/10.1016/j.enconman.2021.114124.

[53] DB Netze. Preisblatt für die nutzung des 16, 7-Hz-bahnstromnetzes (Bahnstromnetz) gültig ab 01.01.2021. URL https://www.dbenergie.de/resource/blob/5816300/29d688b60ee374a7a00ed68b1c84d0e1/Preisblatt-Netznutzung-2021-data.pdf.

[54] Eypasch M, Schimpe M, Kanwar A, Hartmann T, Herzog S, Frank T, et al. Model-based techno-economic evaluation of an electricity storage system based on liquid organic hydrogen carriers. Appl Energy 2017;185:320–30. http://dx.doi.org/10.1016/j.apenergy.2016.10.068.

[55] Kleen G, Padgett E. Durability-adjusted fuel cell system cost: DOE hydrogen program record. 2021, URL https://www.hydrogen.energy.gov/pdfs/21001-durability-adjusted-fcs-cost.pdf,

[56] Jun Tan L, Yang C, Zhou N. Thermoeconomic optimization of a solid oxide fuel cell and proton exchange membrane fuel cell hybrid power system. J Fuel Cell Sci Technol 2014;11(1). http://dx.doi.org/10.1115/1.4025357.

[57] Sakellaris K. Stratetic research and innovation agenda 2021–2027: Clean hydrogen JU SRIA - approved by GB - clean for publication (ID 13246486). 2022, URL https://www.clean-hydrogen.europa.eu/about-us/key-documents/strategic-research-and-innovation-agenda_en,

[58] SOFC reaches 11 years in Jülich lifetime test. Fuel Cells Bull 2019;2019(3):14. http://dx.doi.org/10.1016/S1464-2859(19)30125-7.

[59] Reuß M. Techno-ökonomische analyse alternativer wasserstoffinfrastruktur (Ph.D. thesis), Aachen: RWTH Aachen; 2019.

[60] Nemeth T, Schröer P, Kuipers M, Sauer DU. Lithium titanate oxide battery cells for high-power automotive applications — Electro-thermal properties, aging behavior and cost considerations. J Energy Storage 2020;31:101656. http://dx.doi.org/10.1016/j.est.2020.101656.

[61] Reuß M, Grube T, Robinius M, Preuster P, Wasserscheid P, Stolten D. Seasonal storage and alternative carriers: A flexible hydrogen supply chain model. Appl Energy 2017;200:290–302. http://dx.doi.org/10.1016/j.apenergy.2017.05.050.

[62] yahoo! finance. EUR/USD: Historical data. URL https://finance.yahoo.com/quote/EURUSD%3DX/history?p=EURUSD%3DX.

[63] Hydrogenics. HyPM HD 180. URL https://pdf.directindustry.com/pdf/hydrogenics/hypm-hd-180/33492-420321.html.

[64] Whiston MM, Azevedo IL, Litster S, Whitefoot KS, Samaras C, Whitacre JF. Expert assessments of the cost and expected future performance of proton exchange membrane fuel cells for vehicles. Proc Natl Acad Sci USA 2019;116(11):4899–904. http://dx.doi.org/10.1073/pnas.1804221116.

[65] Leah RT, Bone A, Hammer E, Selcuk A, Rahman M, Clare A, et al. Development progress on the ceres power steel cell technology platform: Further progress towards commercialization. ECS Trans 2017;78(1):87–95. http://dx.doi.org/10.1149/07801.0087ecst.

[66] Woody M, Arbabzadeh M, Lewis GM, Keoleian GA, Stefanopoulou A. Strategies to limit degradation and maximize Li-ion battery service lifetime — Critical review and guidance for stakeholders. J Energy Storage 2020;28:101231. http://dx.doi.org/10.1016/j.est.2020.101231.

[67] Wille N, Pfaff R, Nolte R, Vetter M, Hohn M, Tappert T. Innovatives triebfahrzeug - abschlussbericht. 2020, URL https://bmdv.bund.de/SharedDocs/DE/Anlage/E/innovatives-triebfahrzeug-abschlussbericht.pdf?_blob=publicationFile,

[68] Kadar J, Gackstatter F, Ortner F, Wagner L, Willer M, Preuster P, et al. Boosting power density of hydrogen release from LOHC systems by an inverted fixed-bed reactor design. Int J Hydrog Energy 2024;59:1376–87. http://dx.doi.org/10.1016/j.ijhydene.2024.02.096.

[69] Din T, Hillmansen S. Energy consumption and carbon dioxide emissions analysis for a concept design of a hydrogen hybrid railway vehicle. IET Electr Syst Transp 2018;8(2):112–21. http://dx.doi.org/10.1049/iet-est.2017.0049.

[70] Caponi R, Monforti Ferrario A, Del Zotto L, Bocci E. Hydrogen refueling station cost model applied to five real case studies for fuel cell buses. E3S Web Conf 2021;312:07010. http://dx.doi.org/10.1051/e3sconf/202131207010.

[71] Pelaez J, Davies A. Linde inaugurates world's first hydrogen refueling system for passenger trains. 2022, URL https://www.linde.com/news-media/press-releases/2022/linde-inaugurates-world-s-first-hydrogen-refueling-system-for-passenger-trains,

[72] Rüde T, Dürr S, Preuster P, Wolf M, Wasserscheid P. Benzyltoluene/perhydro benzyltoluene – pushing the performance limits of pure hydrocarbon liquid organic hydrogen carrier (LOHC) systems. Sustain Energy Fuels 2022;6(6):1541–53. http://dx.doi.org/10.1039/D1SE01767E.

[73] Bong B, Mebrahtu C, Jurado D, Bösmann A, Wasserscheid P, Palkovits R. Hydrogen loading and release potential of the LOHC system benzyltoluene/perhydro benzyltoluene over S–Pt/TiO 2 Catalyst. ACS Eng Au 2024;4(3):359–67. http://dx.doi.org/10.1021/acsengineeringau.4c00003.

[74] Siegert F, Gundermann M, Maurer L, Hahn S, Hofmann J, Distel M, et al. Autothermal hydrogen release from liquid organic hydrogen carrier systems. Int J Hydrog Energy 2024;91:834–42. http://dx.doi.org/10.1016/j.ijhydene.2024.10.044.